Distinct interferon signatures and cytokine patterns define additional systemic autoinflammatory diseases

Adriana A. de Jesus,[1] Yangfeng Hou,[2] Stephen Brooks,[3] Louise Malle,[4] Angelique Biancotto,[5] Yan Huang,[1] Katherine R. Calvo,[6] Bernadette Marrero,[7] Susan Moir,[8] Andrew J. Oler,[9] Zuoming Deng,[3] Gina A. Montealegre Sanchez,[1] Amina Ahmed,[10,11] Eric Allenspach,[10,12] Bita Arabshahi,[10,13] Edward Behrens,[10,14] Susanne Benseler,[10,15] Liliana Bezrodnik,[10,16] Sharon Bout-Tabaku,[10,17] AnneMarie C. Brescia,[10,18] Diane Brown,[10,19] Jon M. Burnham,[10,14] Maria Soledad Caldirola,[10,16] Ruy Carrasco,[10,20] Alice Y. Chan,[10,21] Rolando Cimaz,[10,22] Paul Dancey,[10,23] Jason Dare,[10,24] Marietta DeGuzman,[10,25] Victoria Dimitriades,[10,26] Ian Ferguson,[10,27] Polly Ferguson,[10,28] Laura Finn,[10,29] Marco Gattorno,[10,30] Alexei A. Grom,[10,31] Eric P. Hanson,[10,32] Philip J. Hashkes,[10,33] Christian M. Hedrich,[10,34] Ronit Herzog,[10,35] Gerd Horneff,[10,36] Rita Jerath,[10,37] Elizabeth Kessler,[10,38] Hanna Kim,[10,39] Daniel J. Kingsbury,[10,40] Ronald M. Laxer,[10,41] Pui Y. Lee,[10,42] Min Ae Lee-Kirsch,[10,43] Laura Lewandowski,[10,44] Suzanne Li,[10,45] Vibke Lilleby,[10,46] Vafa Mammadova,[10,47] Lakshmi N. Moorthy,[10,48] Gulnara Nasrullayeva,[10,47] Kathleen M. O'Neil,[10,32] Karen Onel,[10,49] Seza Ozen,[10,50] Nancy Pan,[10,49] Pascal Pillet,[10,51] Daniela G.P. Piotto,[10,52] Marilynn G. Punaro,[10,53] Andreas Reiff,[10,54] Adam Reinhardt,[10,55] Lisa G. Rider,[10,56] Rafael Rivas-Chacon,[10,57] Tova Ronis,[10,58] Angela Rösen-Wolff,[10,43] Johannes Roth,[10,59] Natasha Mckerran Ruth,[10,60] Marite Rygg,[10,61] Heinrike Schmeling,[10,15] Grant Schulert,[10,31] Christiaan Scott,[10,62] Gisella Seminario,[10,16] Andrew Shulman,[10,63] Vidya Sivaraman,[10,64] Mary Beth Son,[10,65] Yuriy Stepanovskiy,[10,66] Elizabeth Stringer,[10,67] Sara Taber,[10,68] Maria Teresa Terreri,[10,52] Cynthia Tifft,[10,69] Troy Torgerson,[10,12] Laura Tosi,[10,70] Annet Van Royen-Kerkhof,[10,71] Theresa Wampler Muskardin,[10,72] Scott W. Canna,[73] and Raphaela Goldbach-Mansky[1]

[1]Translational Autoinflammatory Diseases Section (TADS), NIAID/NIH, Bethesda, Maryland, USA. [2]Department of Rheumatology, Shandong Provincial Qianfoshan Hospital, Shandong University, Shandong, China. [3]Biomining and Discovery Section, NIAMS/NIH, Bethesda, Maryland, USA. [4]Icahn School of Medicine at Mount Sinai, New York, New York, USA. [5]Immunology & Inflammation Research Therapeutic Area, Sanofi, Boston, Massachusetts, USA. [6]Department of Laboratory Medicine (DLM), Clinical Center/NIH, Bethesda, Maryland, USA. [7]Computational Systems Biology Section, [8]Laboratory of Immunoregulation, and [9]Bioinformatics and Computational Biosciences Branch (BCBB), Office of Cyber Infrastructure and Computational Biology (OCICB), NIAID/NIH, Bethesda, Maryland, USA. [10]The Autoinflammatory Diseases Consortium, [11]Levine Children's Hospital, Charlotte, North Carolina, USA. [12]Divisions of Immunology & Rheumatology, Department of Pediatrics, University of Washington and Seattle Children's Hospital, Seattle, Washington, USA. [13]Virginia Commonwealth University & Pediatric Specialists of Virginia, Fairfax, Virginia, USA. [14]Division of Rheumatology, Children's Hospital of Philadelphia and the Perelman School of Medicine at the University of Pennsylvania, Philadelphia, Pennsylvania, USA. [15]Department of Pediatrics, Pediatric Rheumatology Section, Alberta Children's Hospital, University of Calgary, Calgary, Alberta, Canada. [16]Immunology Unit, Pediatric Hospital R. Gutierrez, Buenos Aires, Argentina. [17]Department of Pediatric Medicine, Sidra Medicine, Qatar Foundation, Doha, Qatar. [18]Nemours/Alfred I. DuPont Hospital for Children, Wilmington, Delaware, USA. [19]Division of Rheumatology, Children's Hospital Los Angeles & USC, Los Angeles, California, USA. [20]Pediatric Rheumatology, Dell Children's Medical Center of Central Texas, Austin, Texas, USA. [21]Divisions of Pediatric AIBMT & Rheumatology, UCSF, San Francisco, California, USA. [22]Department of Clinical Sciences and Community Health, University of Milano, Milan, Italy. [23]Division of Rheumatology, Janeway Children's Hospital & Rehabilitation Centre, Saint John's, Newfoundland and Labrador, Canada. [24]Division of Pediatric Rheumatology, University of Arkansas for Medical Sciences, Arkansas Children's Hospital, Little Rock, Arkansas, USA. [25]Department of Immunology, Allergy and Rheumatology, Baylor College of Medicine, Houston, Texas, USA. [26]Division of Pediatric Allergy, Immunology & Rheumatology, UC Davis Health, Sacramento, California, USA. [27]Department of Pediatrics/Pediatric Rheumatology, Yale University School of Medicine, New Haven, Connecticut, USA. [28]Pediatrics Department, University of Iowa Carver College of Medicine, Iowa City, Iowa, USA. [29]Pathology Department, University of Washington and Seattle Children's Hospital, Seattle, Washington, USA. [30]Center for Autoinflammatory Diseases and Immunedeficiencies, IRCCS Giannina Gaslini, Genoa, Italy. [31]Division of Rheumatology, Children's Hospital Medical Center, Cincinnati, Ohio, USA. [32]Department of Pediatrics Indiana University School of Medicine and Riley Hospital for Children, Indianapolis, Indiana, USA. [33]Pediatric Rheumatology Unit, Shaare Zedek Medical Center, Jerusalem, Israel. [34]Department of Women's & Children's Health, Institute of Translational Medicine, University of Liverpool & Department of Paediatric Rheumatology, Alder Hey Children's NHS Foundation Trust Hospital, Liverpool, United Kingdom. [35]Department of Otolaryngology, Division of Allergy and Immunology, New York University, New York, New York, USA. [36]Asklepios Klinik Sankt, Augustin GmbH, St. Augustin, Germany and Department of Pediatric and Adolescents Medicine, University of Cologne, Cologne, Germany. [37]Augusta University Medical Center, Augusta, Georgia, USA. [38]Division of Rheumatology, Children's Mercy, Kansas City and University of Missouri, Kansas City, Missouri, USA. [39]Pediatric Translational Research Branch, NIAMS/NIH, Bethesda, Maryland, USA. [40]Randall Children's Hospital at Legacy Emanuel, Portland, Oregon, USA. [41]Division of Pediatric Rheumatology, University of Toronto and The Hospital for Sick Children, Toronto, Ontario, Canada. [42]Division of Allergy, Immunology and Rheumatology, Boston Children's Hospital, Boston, Massachusetts, USA. [43]Department of Pediatrics, Medizinische Fakultät Carl Gustav Carus, Technische Universität Dresden, Dresden, Germany. [44]Systemic Autoimmunity Branch, NIAMS/NIH, Bethesda, Maryland, USA. [45]Hackensack University Medical Center, Hackensack Meridian School of Medicine at Seton Hall University, Hackensack, New Jersey, USA. [46]Department of Rheumatology, Pediatric Section, Oslo University Hospital, Oslo, Norway. [47]Azerbaijan Medical University, Baku, Azerbaijan. [48]Rutgers - Robert Wood Johnson Medical School, New Brunswick, New Jersey, USA. [49]Division of Pediatric Rheumatology, Weill Cornell Medicine & Hospital for Special Surgery, New York, New York, USA. [50]Hacettepe University, Department of Pediatrics, Ankara, Turkey. [51]Children Hospital Pellegrin-Enfants, Bordeaux, France. [52]Department of Pediatric Rheumatology, Federal University of Sao Paulo, Sao Paulo, Brazil. [53]Department of Pediatrics, University of Texas Southwestern Medical Center, Dallas, Texas, USA. [54]Division of Rheumatology, Children's Hospital Los Angeles, Keck School of Medicine, USC, Los Angeles, California, USA. [55]University of Nebraska Medical Center/Children's Hospital and Medical Center, Omaha, Nebraska, USA. [56]Environmental Autoimmunity Group, NIEHS/NIH, Bethesda, Maryland, USA. [57]Department of Pediatric Rheumatology, Nicklaus Children's Hospital, Miami, Florida, USA. [58]Division of Pediatric Rheumatology, Children's National Health System, Washington, DC, USA. [59]Division of Pediatric Dermatology and Rheumatology, Children's Hospital of Eastern Ontario, Ottawa, Canada. [60]Medical University of South Carolina, Charleston, South Carolina, USA. [61]Department of Clinical and Molecular Medicine, NTNU - Norwegian University of Science and Technology, and Department of Pediatrics, St. Olavs Hospital, Trondheim, Norway. [62]University of Cape Town, Red Cross War Memorial Children's Hospital, Cape Town, South Africa. [63]Pediatric Rheumatology, Children's Hospital of Orange County, UC Irvine, Irvine, California, USA. [64]Section of Rheumatology, Nationwide Children's Hospital, Columbus, Ohio, USA. [65]Division of Immunology, Boston Children's Hospital, Boston, Massachusetts, USA. [66]Department of Pediatric Infectious Diseases and Immunology, Shupyk National Medical Academy for Postgraduate Education, Kiev, Ukraine. [67]IWK Health Centre, Dalhousie University, Halifax, Nova Scotia, Canada. [68]Division of Pediatric Rheumatology, Department of Rheumatology, Hospital for Special Surgery, New York, New York, USA. [69]Undiagnosed Diseases Program, NHGRI/NIH, Bethesda, Maryland, USA. [70]Bone Health Program, Children's National Health System, Washington, DC, USA. [71]Department of Pediatric Immunology and Rheumatology, Wilhelmina Children's Hospital Utrecht, Utrecht, Netherlands. [72]New York University School of Medicine, New York, New York, USA. [73]Children's Hospital Pittsburgh, Pittsburgh, Pennsylvania, USA.

BACKGROUND. Undifferentiated systemic autoinflammatory diseases (USAIDs) present diagnostic and therapeutic challenges. Chronic interferon (IFN) signaling and cytokine dysregulation may identify diseases with available targeted treatments.

METHODS. Sixty-six consecutively referred USAID patients underwent underwent screening for the presence of an interferon signature using a standardized type-I IFN-response-gene score (IRG-S), cytokine profiling, and genetic evaluation by next-generation sequencing.

RESULTS. Thirty-six USAID patients (55%) had elevated IRG-S. Neutrophilic panniculitis (40% vs. 0%), basal ganglia calcifications (46% vs. 0%), interstitial lung disease (47% vs. 5%), and myositis (60% vs. 10%) were more prevalent in patients with elevated IRG-S. Moderate IRG-S elevation and highly elevated serum IL-18 distinguished 8 patients with pulmonary alveolar proteinosis (PAP) and recurrent macrophage activation syndrome (MAS). Among patients with panniculitis and progressive cytopenias, 2 patients were compound heterozygous for potentially novel *LRBA* mutations, 4 patients harbored potentially novel splice variants in *IKBKG* (which encodes NF-κB essential modulator [NEMO]), and 6 patients had de novo frameshift mutations in *SAMD9L*. Of additional 12 patients with elevated IRG-S and CANDLE-, SAVI- or Aicardi-Goutières syndrome–like (AGS-like) phenotypes, 5 patients carried mutations in either *SAMHD1*, *TREX1*, *PSMB8*, or *PSMG2*. Two patients had anti-MDA5 autoantibody–positive juvenile dermatomyositis, and 7 could not be classified. Patients with *LRBA*, *IKBKG*, and *SAMD9L* mutations showed a pattern of IRG elevation that suggests prominent NF-κB activation different from the canonical interferonopathies CANDLE, SAVI, and AGS.

CONCLUSIONS. In patients with elevated IRG-S, we identified characteristic clinical features and 3 additional autoinflammatory diseases: IL-18–mediated PAP and recurrent MAS (IL-18PAP-MAS), NEMO deleted exon 5–autoinflammatory syndrome (NEMO-NDAS), and SAMD9L-associated autoinflammatory disease (SAMD9L-SAAD). The IRG-S expands the diagnostic armamentarium in evaluating USAIDs and points to different pathways regulating IRG expression.

TRIAL REGISTRATION. ClinicalTrials.gov NCT02974595.

FUNDING. The Intramural Research Program of the NIH, NIAID, NIAMS, and the Clinical Center.

Conflict of interest: RGM received investigator-initiated grants under government collaborative agreements from SOBI, Lilly, Regeneron and Novartis. SWC received grants from Novartis and AB2Bio. JAD received grants from Pfizer, Roche, and Bristol-Myers Squibb. AAG received grants from NovImmune, grants and personal fees from Ab2Bio, and grants from Novartis. RML received consultant fees from SOBI and Novartis. LGR received research support from Hope Pharmaceuticals, Bristol-Myers Squibb, and Elli Lily. GS received personal fees from Novartis. TLWM received grants from Arthritis National Research Foundation, NYU Clinical & Translational Science Institute; personal fees from Novartis; and has a patent Methods and Materials for Treating Autoimmune Conditions issued.
Copyright: © 2020, American Society for Clinical Investigation.
Submitted: April 2, 2019; **Accepted:** December 18, 2019; **Published:** February 24, 2020.
Reference information: *J Clin Invest*. 2020;130(4):1669–1682. https://doi.org/10.1172/JCI129301.

Introduction

The discovery of Mendelian defects that cause immune-dysregulatory and autoinflammatory diseases rapidly expanded our ability to diagnose pediatric patients with systemic sterile inflammation and provided insights into pathogenic mechanisms that cause organ inflammation and damage. Furthermore, pathogenesis and treatment studies in autoinflammatory diseases converge on confirming a key role of proinflammatory cytokines in amplifying abnormal immune responses, which have become effective targets for treatments (1).

Mutations in IL-1–activating inflammasomes (including NLRP3 and pyrin) and their remarkable response to IL-1–inhibiting therapies suggest a central role for IL-1 in their pathogenesis (1). More recently, 2 diseases with systemic inflammation, one caused by gain-of-function mutations in the viral sensor *STING1/TMEM173* (STING) causing STING-associated vasculopathy with onset in infancy (SAVI), and another by additive loss-of-function mutations in proteasome genes causing the proteasome-associated autoinflammatory syndromes (PRAAS) (also, chronic atypical neutrophilic dermatosis with lipodystrophy and elevated temperatures [CANDLE]), presented with chronically elevated interferon (IFN) signatures, suggesting a pathogenic role for type-I IFN in autoinflammatory diseases (2, 3). Type-I IFN was first discovered as a soluble antiviral factor over 50 years ago, and a role in sterile inflammation was proposed in patients with systemic lupus erythematosus (4). However, the discovery of genetic mutations that cause the autoinflammatory type-I interferonopathies CANDLE (2, 5), SAVI (3, 6–8), and Aicardi-Goutières syndrome (AGS) (9, 10) have shed light on pathomechanisms that drive chronic IFN signaling, and recent studies blocking IFN signaling validate a critical role for type-I IFNs (11). AGS-causing loss-of-function mutations in nucleases impair self–nucleic acid homeostasis, SAVI-causing

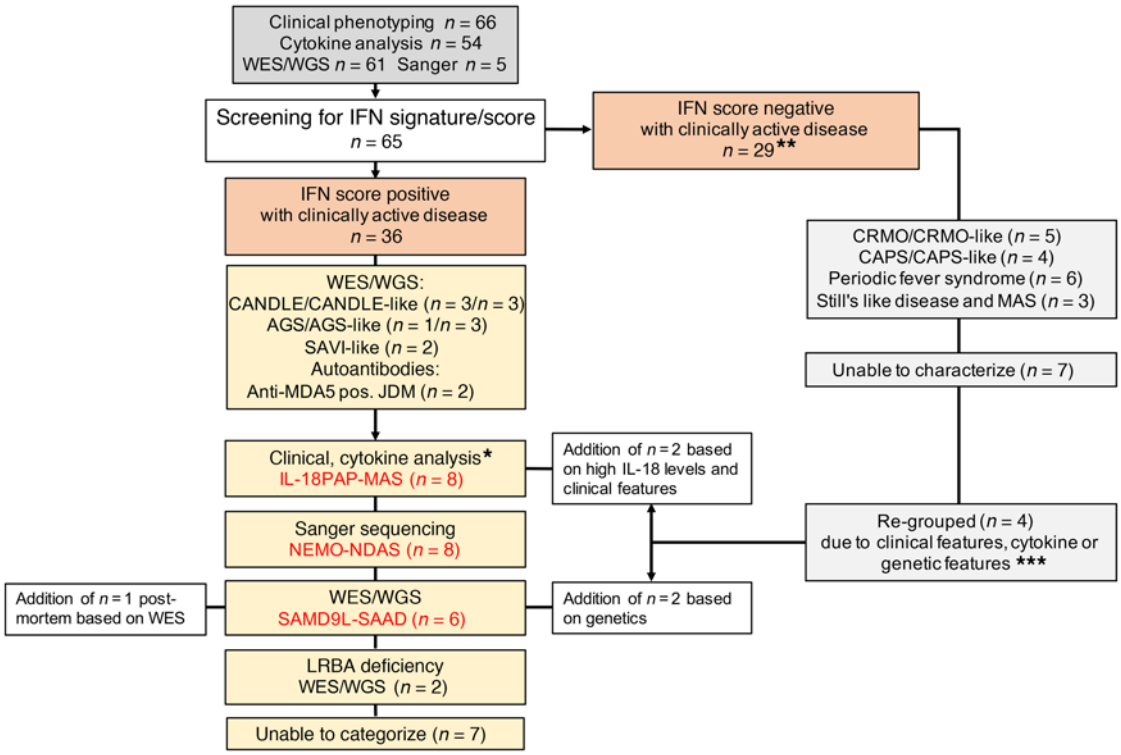

Figure 1. Study overview, patient allocation and diagnosis. All patients were screened for elevation of an IFN-response-gene score (IRG-S) except for 1 patient (G4-P5), who was diagnosed postmortem based on WES with SAMD9L-SAAD. Patients were characterized based on presence or absence of an elevated IRG-S. All patients underwent clinical phenotyping, cytokine analyses, and genetic testing (WES/WGS or Sanger sequencing). Negative–IRG-S patients were clinically grouped (see supplement). Positive–IRG-S patients were grouped as CANDLE-like, SAVI-like, and AGS-like disease. Cytokine analyses and genetic analyses allowed for the characterization of patients with 3 additional diseases: IL-18PAP-MAS, NEMO-NDAS, and SAMD9L-SAAD (in red); and 2 patients had LRBA deficiency. Three patients had CANDLE, 1 AGS5, and 2 had anti-MDA5 autoantibody positive juvenile dermatomyositis. Seven patients with an elevated IRG-S and 7 patients with negative IRG-S could not be further classified. *No monogenic candidate gene. **Negative–IRG-S patients were classified as CRMO/CRMO-like (n = 5), CAPS/CAPS-like (n = 4), periodic fever syndrome (n = 6), Still's-like disease and MAS (n = 3); 7 patients could not be classified. ***Two patients (G1-P5 and G4-P6) only had one sample, 1 patient (G4-P3) had a bone marrow transplant (BMT) and no pre-BMT sample available, and 1 patient (G1-P3) had 3 negative samples.

gain-of-function mutations in *STING1/TMEM173* lead to chronic predominantly IFN-β production, and PRAAS-causing loss-of-function mutations in proteasome genes cause an elevated IFN signature that is independent of nucleic acids and viral sensor activation and points to additional intracellular mechanisms that trigger an IFN signature.

A link between autoinflammation and type-II IFN (IFN-γ) was recently established via the discovery of gain-of-function mutations in *NLRC4* (12, 13). Patients demonstrate chronically and extremely high levels of serum IL-18, as well as evidence for IFN-γ activity during flares (14). Highly elevated serum IL-18 levels emerged as risk factors for developing macrophage activation syndrome (MAS) and have been associated with the development of MAS in systemic juvenile idiopathic arthritis and adult-onset Still's disease (15, 16). The disease-causing *NLRC4* mutations have associated the NLRC4 inflammasome but not the other inflammasomes with very high IL-18 activation (15). Mutations in *XIAP* (17) and *CDC42* (18) are other monogenic autoinflammatory syndromes with high IL-18 levels that predispose to the development of MAS, thus providing genetically defined disease models to study the role of IL-18 in MAS. The presence of free IL-18 in these patients with ultrahigh serum IL-18 levels may modify the synergy with IL-12 in promoting the production of the type-II IFN, IFN-γ (19), which emerges as the critical factor in leading to the hyperinflammatory state of MAS (14).

Emerging data from interventional studies targeting the type-I IFN and IL-18/type-II IFN pathways have shown benefit in patients with these diseases and treatment also might benefit patients who currently have no genetic diagnosis but evidence of immune dysregulation in the respective inflammatory pathways. Patients with chronically elevated IFN signatures may clinically respond to treatments that block type-I IFN signaling (11). Likewise, patients with high serum IL-18 levels and an MAS predisposition might respond to treatments that target IL-18 (20) and/or the type-II IFN, IFN-γ (21).

Comprehensive clinical phenotyping of undifferentiated systemic autoinflammatory disease (USAID) patients and screening for an IFN signature by using a standardized type-I IFN response gene score (IRG-S), a targeted cytokine profile, and by genomic evaluation, led to the identification of 3 additional autoinflammatory diseases, IL-18–associated pulmonary alveolar proteinosis (PAP) and MAS syndrome (IL-18PAP-MAS), NEMO deleted exon 5–autoinflammatory syndrome (NEMO-NDAS), and SAMD9L-associated autoinflammatory disease (SAMD9L-SAAD). The pref-

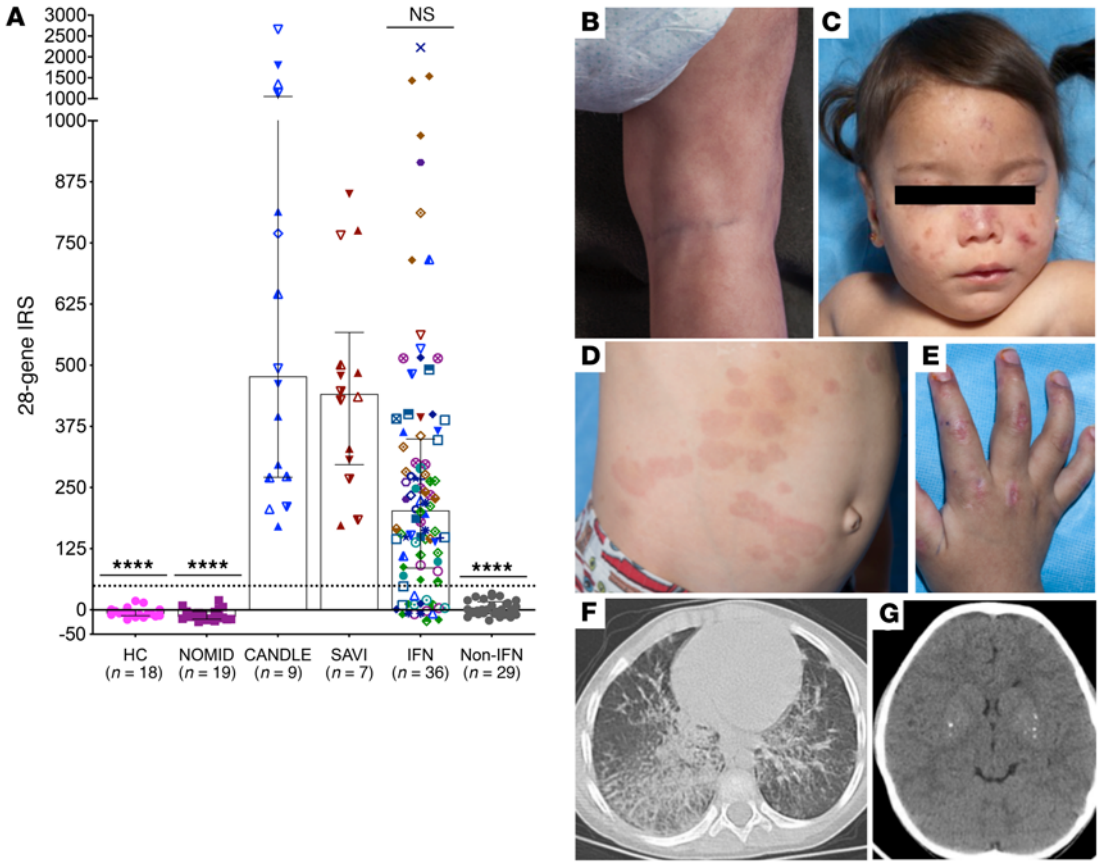

Figure 2. Shared clinical features and different cytokine profiles in patients with and without elevated IFN scores. (**A**) An elevated IFN-response gene score (IRG-S) distinguishes 36 patients during active disease from 29 patients who had normal IFN scores during bouts of active disease. Nonparametric (Kruskal-Wallis) test was used for multiple comparisons of IFN or Non-IFN groups with healthy controls (HC) or with CANDLE and SAVI patients combined. Depicted in the graph are the statistical significances (Kruskal-Wallis test) from the comparisons of each group (NOMID, IFN, and Non-IFN groups) with CANDLE and SAVI patients combined. Each individual patient is represented by a different symbol shape. ****$P < 0.0001$; NS, not significant. Bars and error lines indicate median and interquartile range, respectively; dotted line indicates the 28-gene IFN score cutoff (48.9) previously described (34). Multiple comparisons of each group (NOMID, CANDLE, and SAVI combined; IFN and Non-IFN) with HC (not depicted): NOMID $P = 0.5004$, CANDLE + SAVI $P < 0.0001$, IFN $P < 0.0001$, Non-IFN $P = 0.2986$. For HC, NOMID, and non-IFN groups, the same symbol is used for different individuals, as only 1 sample per patient is included. For CANDLE, SAVI, and IFN groups, each patient is represented by a different symbol. (**B**–**G**) Characteristic clinical features that were present only in patients with elevated IFN scores included panniculitis with lipoatrophy (**B**), neutrophilic vasculitis (**C**), erythematous macular rash (**D**), Gottron's papules (**E**), interstitial lung disease (**F**), and basal ganglia calcifications (**G**). Four patients (per groups defined in Table 2; Group 1 – patient 3 [G1-P3] and G1-P5, G4-P2 and G4-P5) had negative IRG-S but were later added to the respective groups when a clinical or genetic diagnosis was made (not depicted).

erential elevation of IFN-response genes (IRGs) with STAT-1 and NF-κB binding sites in patients with NEMO-NDAS, LPS-responsive beige-like anchor protein (LRBA) deficiency, and SAMD9L-SAAD suggests a prominent role for both NF-κB and IFN signaling, which is distinct from CANDLE, SAVI, and AGS.

Results

Screening by using a validated IFN response gene score (IRG-S) identifies distinct clinical features in patients with elevated IRG-S compared with patients with normal IRG-S. IRG expression is low in healthy controls and untreated patients with the IL-1–mediated disease, neonatal-onset multisystem inflammatory disease (NOMID), and elevated in patients with PRAAS/CANDLE and SAVI. Of 65 patients tested for IRG-S elevation (see workflow in Figure 1), 36 (55%) had elevated IRG-S with an active disease flare and 29 patients were negative (Figure 2A). Four of the 29 patients with a normal IRG-S at the time of testing were later included in one of the disease groups of patients with an elevated IRG-S during disease flares (Table 1 and Supplemental Table 1; supplemental material available online with this article; https://doi.org/10.1172/JCI129301DS1). Clinical and laboratory features varied in patients with and without elevated IRG-S and a significantly earlier disease onset was observed in patients with elevated IRG-S (Figure 2, B–G, Table 1, and Supplemental Table 1). Panniculitis was present in 22 patients (54%) included in disease groups with an elevated IRG-S, compared with no patient with a normal IRG-S ($P < 0.0001$). Similarly, basal ganglia calcifications were present in 12 out of 26 patients (46%) with elevated IRG-S who had either CTs or MRIs compared with none of 14 patients with normal IRG-S ($P < 0.01$). Other clinical features that were more frequent in patients with elevated IRG-S included interstitial lung disease (47% vs. 5% in patients with normal IRG-S), myositis (60% vs. 10% with normal IRG-S), arterial hypertension (30% vs. 4% with normal IRG-S), and liver enzyme elevation (61% vs. 12% with normal IRG-S) (Table 1).

Table 1. Clinical features of genetically defined type-I interferonopathies and noninterferonopathies

	Clinical Feature	With IFN signature affected/no. patients evaluated (%) *n* = 41[A]	Without IFN signature affected/no. patients evaluated (%) *n* = 25	Fisher's exact test *P* value
Demographics	Age of disease onset (median [IQR]), months[B]	6 (0–15)	24 (1.5–57)	**0.009**[G]
	Age of disease onset < 2 yr	31/41 (75)	12/25 (48)	**0.033**
	Female	24/41 (58)	11/25 (44)	NS
	White	21/41 (51)	21/25 (84)	**0.009**
	Mortality[C]	8/41 (19.5)	0/25 (0)	**0.020**
Skin	Any rash	37/39	17/25	**0.010**
	Panniculitis with or without lipodystrophy	22/41 (54)	0/25 (0)	**<0.0001**
	Pustulosis	2/41 (5)	3/25 (12)	NS
	Pyoderma gangrenosum	1/41 (2.4)	1/25 (4)	NS
Neurologic	Basal ganglia calcifications	12/26 (46)	0/14 (0)	**0.003**
	Demyelinating disease[D]	7/25 (28)	1/14 (7)	NS
	Aseptic meningitis[E]	3/28 (11)	1/22 (4.5)	NS
Pulmonary	Interstitial lung disease with or without clubbing[F]	18/38 (47)	1/19 (5.3)	**0.002**
Musculoskeletal	Myositis[H]	21/35 (60)	2/19 (10)	**0.0005**
	Aseptic osteomyelitis	1/40 (2.5)	6/19 (32)	**0.010**
Vascular	Skin vasculitis	10/40 (25)	2/25 (8)	NS
	Stroke	2/37 (5.4)	1/25 (4)	NS
	Arterial hypertension	10/33 (30)	1/25 (4)	**0.016**
	Vascular calcification	5/33 (15)	0/19 (0)	NS
Liver disease	Transaminitis	23/38 (61)	3/25 (12)	**0.0002**
	Abnormal liver biopsy[I]	7/38 (16)	1/25 (4)	NS
Other	MAS	11/39 (28)	2/25 (8)	0.062

[A]For clinical phenotyping, 4 patients (G1-P3, G1-P5, G4-P3, and G4-P6) were negative and 1 patient (G4-P5) did not have an IFN-response-gene score (IRG-S) tested but were later added to the respective groups when clinical or genetic diagnosis was made. The final number of subjects in the group of patients with a diagnosis related to a "positive" IRG-S (with IFN signature) was 41, and 25 patients were listed with "negative" IRG-S (without IFN signature). [B]Two patients in this group had disease onset above 18 years old and were excluded from the analysis. [C]One patient with SAMD9L-associated autoinflammatory disease (SAMD9L-SAAD) was diagnosed postmortem (G4-P5). [D]Patients with magnetic resonance imaging (MRI). [E]Patients with lumbar puncture. [F]Patients with chest computed tomography. [G]Unpaired *t* test was performed. [H]Myositis was defined as elevated creatine kinase or aldolase and/or abnormal muscle MRI. [I]Undifferentiated interferonopathy (UIFN) group: histiocyte infiltration (*n* = 1) (G1-P3); granulomatous hepatitis (*n* = 2) (G2-P1 and G3-P1); autoimmune hepatitis with liver fibrosis (*n* = 1) (G2-P2); nodular regenerative hyperplasia (*n* = 1) (G5-P3); ballooning and necrosis of hepatocytes (*n* = 2) (G6-P1 and G6-P2); and periportal fibrosis (*n* = 1) (G6-P1). Noninterferonopathy (Non-IFN) group: liver fibrosis and vanishing bile duct disease (*n* = 1) (GN5-P3). Features with *P* values in bold were significantly different between patients with and without IFN signatures.

On laboratory evaluation (Supplemental Table 2), lymphopenia (with low B cell and NK cell counts) and thrombocytopenia were present in 24%–31% of patients with elevated IRG-S compared with none with normal IRG-S; patients with high IRG-S were more frequently anemic (36% vs. 8%). Antinuclear antibodies were present in patients with and without an elevated IRG-S (33% vs. 11%, *P* = nonsignificant) but were more prevalent in patients with an elevated IRG-S; anti-dsDNA antibodies and anti-neutrophil antibodies (anti-PR3 and anti-MPO) were low positive in 1 or 2 patients with an elevated IRG-S each. In contrast, autoantibodies against endothelial lipoproteins (anti-cardiolipin, lupus anticoagulant) were equally positive in patients with and without elevated IRG-S. Serum IgA and IgM levels were higher in patients with elevated IRG-S (Supplemental Table 2).

Mortality within the study period was high in patients with positive IRG-S: 8 out of 41 (19.5%) expired within the study period (2014 to 2018); all patients with normal IRG-S are alive (Table 1). The IRG-S elevation was thought to be associated with active disease, although absence of infection could not always be excluded as a contributing factor to the increased IRG-S.

Of the 41 patients in the disease groups with elevated IRG-S, 18 were diagnosed with additional diseases based on clinical phenotype, cytokine and/or genetic analyses, and are described in groups 1 to 4 (G1–G4). Eight patients with PAP and recurrent MAS were grouped into G1. Twelve patients with CANDLE-like features had relatively lower IRG-S with disease flares than patients with CANDLE and were later genetically classified with distinct diseases: LRBA deficiency (G2, *n* = 2), NEMO-NDAS (G3, *n* = 4), and SAMD9L-SAAD (G4, *n* = 6). Several patients with high IRG-S resembled AGS (G5, *n* = 4) and one of them had a known mutation in *SAMHD1*. Two patients with high IRG-S, interstitial lung disease, soft tissue calcifications, and myositis had elevated anti-MDA5 autoantibodies, consistent with anti-MDA5 autoantibody–positive juvenile dermatomyositis (JDM) (G6, *n* = 2). Of the

Table 2. Diagnoses of patients with elevated type-1 IFN score (IRG-S), including genetic and immune evaluation

Disease group	Number of patients in group (*n* = 41)	Disease name	Number of patients with monogenic disease-causing mutation	Presumed genetic mechanism	Possible candidate/modifying genes	Diagnostic approach to a clinical diagnosis [E]
Group 1	*n* = 8	IL-18 PAP-MAS	*n* = 0[A]	poly/oligogenic	none/possible modifying genes	Clinical phenotype and cytokine analysis (high IL-18)
Group 2	*n* = 2	LRBA deficiency	*n* = 2[B]	*LRBA* compound heterozygous, recessive	monogenic/modifying genes	Genetic testing (WES)
Group 3	*n* = 4	NEMO-NDAS	*n* = 4	*IKBKG* encoding NEMO, novel splice site mutations, X-linked	monogenic/none	Genetic testing (WGS)
Group 4	*n* = 6	SAMD9L-SAAD	*n* = 6[C]	*SAMD9L*, de novo frameshift mutations, autosomal dominant	monogenic/none	Genetic testing (WES), trio analysis
Group 5	*n* = 4	AGS/AGS-like	*n* = 1	*SAMHD1*, recessive	1 candidate gene/NA	Genetic testing (WGS)
Group 6	*n* = 2	MYOSITIS plus positive anti-MDA5 autoantibody	*n* = 0	not known	none/possible modifying genes	Clinical phenotype and autoantibody testing
Group 7	*n* = 6	CANDLE/CANDLE-like with panniculitis	*n* = 4[D]	*PSMB8* recessive (*n* = 2); *PSMG2* recessive (*n* = 1); *TREX1* de novo, somatic (n = 1)	2 candidate genes/NA	Genetic testing (WES), trio analysis
Group 8	*n* = 2	SAVI-like	*n* = 0	not known	none/no modifying genes	Clinical phenotyping
Group 9	*n* = 7	Miscellaneous	*n* = 1	variable, not one disease	possible candidates/NA	Clinical phenotyping

[A]One patient was diagnosed with myeloid leukemia after treatment for MAS that included etoposide. [B]Both patients have modifying genes that may influence their phenotype. [C]One patient was included postmortem because of a disease-causing *SAMD9L* mutation that was identical to that in 2 other patients. [D]Three patients have potentially novel proteasome mutations and have CANDLE/PRAAS, and 1 patient had a known *PSMB8* mutation, p.T75M. [E]See Supplemental Table 7 for best-candidate genes.

remaining patients in the disease groups with positive IRG-S, 3 had mutation-positive CANDLE and 3 had CANDLE-like features and were grouped in group 7 (G7, *n* = 6). Of the 3 CANDLE patients, 1 had a known mutation (*n* = 1), and 1 had a potentially novel mutation (*n* = 1) in the CANDLE-causing gene *PSMB8*. The third patient was compound heterozygous for mutations in a potentially novel CANDLE-causing gene, *PSMG2* (*n* = 1). Two patients with SAVI-like features did not have disease-causing mutations and are described in G8 (SAVI-like)(*n* = 2) (see Supplemental Methods for definition of disease categories, Supplemental Methods A). Seven patients, each with clinical features unlike any other patient, could not be grouped or classified (G9, *n* = 7).

We assessed 48 cytokines in 53 patients with available serum samples (Supplemental Figure 1). The median IP-10 levels were significantly higher in patients with an elevated IRG-S (*n* = 20) compared with those with a normal IRG-S (*n* = 25) (7,369 [range 404.1–25,884] vs. 622.1 [191.4–3,185] pg/mL, $P < 0.0001$). Other cytokines that were significantly elevated include MIG/CXCL9 (2,890 [range 441.9–43,205] vs. 737.5 [83.4–1,272] pg/mL, $P = 0.0001$), SCF/KITLG (38.9 [4.3–209.8] vs. 20.9 [3.5–107.2] pg/mL, $P = 0.0156$), GROα/CXCL1 (251.6 [74.9–1,696] vs. 161.7 [24.9–314.8] pg/mL, $P = 0.0043$), and TRAIL (94.8 [18.1–633.3] vs. 47.9 [10.7–290.0] pg/mL, $P = 0.0277$).

Highly elevated serum IL-18 levels, PAP, and recurrent MAS characterize a defined clinical syndrome. Eight patients with a history of recurrent MAS, PAP, and nail clubbing (Figure 3, A–C) had ultrahigh elevations of serum IL-18 levels (Figure 3, D and E). Three were repeatedly tested for the entire cytokine panel and had significantly increased expression of a 12-cytokine signature nearly identical to that seen in patients with an *NLRC4* gain-of-function mutation and recurrent MAS (NLRC4-MAS), which includes hematopoietic growth factors/cytokines like M-CSF, SCF, and IL-3 (12) (Figure 3D). However, whole-exome sequencing (WES) did not reveal definitive candidate mutations and no patient had *NLRC4* mutations. The distinct clinical presentation with PAP, the very high IL-18 levels (Figure 3E), an IL-18/CXCL9 ratio similar to patients with NLRC4-MAS (14) (Figure 3F), and a cytokine signature previously associated with recurrent MAS clinically suggest a previously unrecognized disease, that is subsequently referred to as IL-18–associated PAP and MAS syndrome (IL-18PAP-MAS). These patients are combined in G1. Of the 8 patients, 7 had active disease at the time of assessment and 6 had an elevated IRG-S with active disease, although elevations were significantly lower than in CANDLE and SAVI ($P = 0.0002$ and $P = 0.0003$, respectively) (Figure 4A). In 1 patient with inactive disease and a normal C-reactive protein (CRP) at the time of blood draw, serum IL-18 levels had dropped from 430,423 pg/mL during active disease to 2,506 pg/mL (normal <500 pg/mL) and the IRG-S was normal. This patient was included in G1 due to the clinical phenotype of IL-18PAP-MAS and the ultrahigh IL-18 levels at the time of active disease. Supplemental Table 3 includes the clinical features and treatments for the IL-18PAP-MAS group.

Genetic analyses of 12 patients with CANDLE-like clinical phenotypes including panniculitis, but also progressive B cell lymphopenia, and low/intermediate IRG-S revealed potentially novel mutations in LRBA, potentially novel splice variants in IKBKG/NEMO, and truncating mutations in SAMD9L. Twelve patients with CANDLE-like phenotypes who were negative for known CANDLE-causing mutations had low/intermediate IRG-S and all developed progressive cytopenias. WES identified 2 patients with potentially novel or very

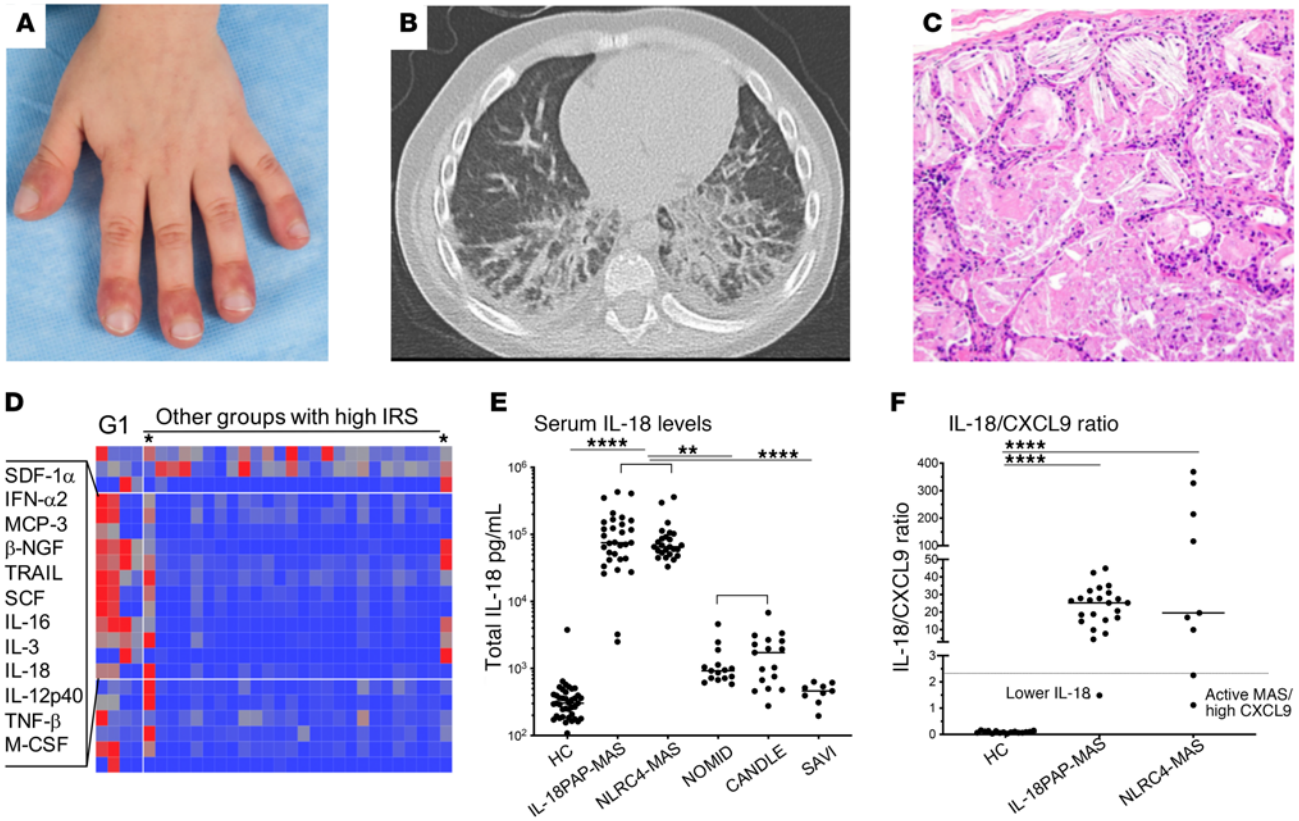

Figure 3. Clinical features and cytokine dysregulation in patients with IL-18PAP-MAS (*n* = 8). (**A**) Nail clubbing. (**B**) Interstitial and alveolar lung disease. (**C**) Histologic features characteristic of pulmonary alveolar proteinosis (PAP). Original magnification, ×20. (**D**) Heatmap of 22 out of 48 analytes tested. The 12-cytokine signature includes SDF-1α/CXCL12, IFN-α2, MCP-3/CCL7, β-NGF, TRAIL, SCF, IL-16, IL-3, IL-18, IL-12p40, TNF-β/Lt α, and M-CSF. The 12-cytokine signature upregulation tracks with ultrahigh IL-18 levels that are also seen in patients with recurrent macrophage activation syndrome (MAS) and gain-of-function mutations in *NLRC4* (12). Two other patients with the 12-cytokine signature (*) had MAS but no pulmonary disease. (**E**) Serum IL-18 levels in patients with IL-18PAP-MAS and healthy and disease controls. HC, healthy controls; IL-18PAP-MAS, G1 patients with PAP and recurrent MAS (*n* = 8); NLRC4/MAS, patients with monogenic NLRC4-mediated MAS (*n* = 5); NOMID, neonatal-onset multisystem inflammatory disease (*n* = 8); SAVI, STING-associated vasculopathy with onset in infancy (*n* = 5); CANDLE, chronic atypical neutrophilic dermatosis with lipodystrophy and elevated temperatures (*n* = 8). (**F**) IL-18/CXCL9 ratio has previously been described to a cutoff of 2.3 (15), which is indicated with a gray horizontal line. IL-18PAP-MAS (*n* = 7); NLRC4/MAS, patients with monogenic NLRC4-mediated MAS (*n* = 5). In **E** and **F**, nonparametric test (Kruskal-Wallis) was performed for multiple comparisons and all significant differences are shown. In **E**, populations in brackets share the same significance pattern. *$P < 0.05$; **$P < 0.01$; ****$P < 0.0001$.

rare compound heterozygous *LRBA* mutations (22). One of the LRBA-deficiency patients (G2-P2) had severe lipoatrophy, hepatomegaly, and type 2 insulin-resistant diabetes (DM type 2). A de novo mutation in *IRS-1* (c.3632T>G; p.L1211R), encoding the insulin receptor substrate 1 previously associated with DM type 2 (23, 24), may have contributed to this phenotype but was not formally evaluated. Upon leptin replacement, the patient's profound DM type 2 and hepatosplenomegaly resolved (25). The patient subsequently developed transverse myelitis and septic arthritis and underwent a bone marrow transplant. The other patient (G2-P1) had recurrent neutrophilic panniculitis in predominantly lower extremities and granulomatous hepatitis (Supplemental Table 4). Both patients were combined in G2 based on their biallelic *LRBA* mutations, reduced surface expression of CTLA4, and reduced number of regulatory T cells, consistent with previous findings in patients with LRBA deficiency (26) (data not shown).

One patient with lymphohistiocytic panniculitis and chorioretinitis (G3-P1) had conical teeth reminiscent of the ectodermal dysplasia found in NEMO deficiency syndrome, which prompted targeted sequencing of *IKBKG* (the causative gene in NEMO deficiency), the gamma subunit of the IκB kinase complex that regulates NF-κB activation. This patient, 2 other males, and 1 girl with panniculitis, progressive B cell lymphopenia, and hypogammaglobulinemia all had de novo splice-site variants that lead to deletion of exon 5 of *IKBKG* (G3-P1 to G3-P4) and are listed under G3 (Supplemental Table 4).

Genetic evaluation of 6 other patients revealed 3 tightly clustered de novo frameshift mutations in *SAMD9L*. All patients were clinically diagnosed as CANDLE due to the prominent neutrophilic panniculitis that was clinically and histologically indistinguishable from CANDLE. However, 4 patients also had early-onset, severe interstitial lung disease, a clinical feature that is not seen in CANDLE (Figure 4B). These patients had lower IRG-S in the context of high CRPs than CANDLE patients and developed progressive isolated B cell and NK cell cytopenias (Supplemental Table 4). One patient, who succumbed from respiratory failure at the age of 2 months, was included postmortem; she and 2 other patients had the identical de novo frameshift mutations in *SAMD9L*. Two

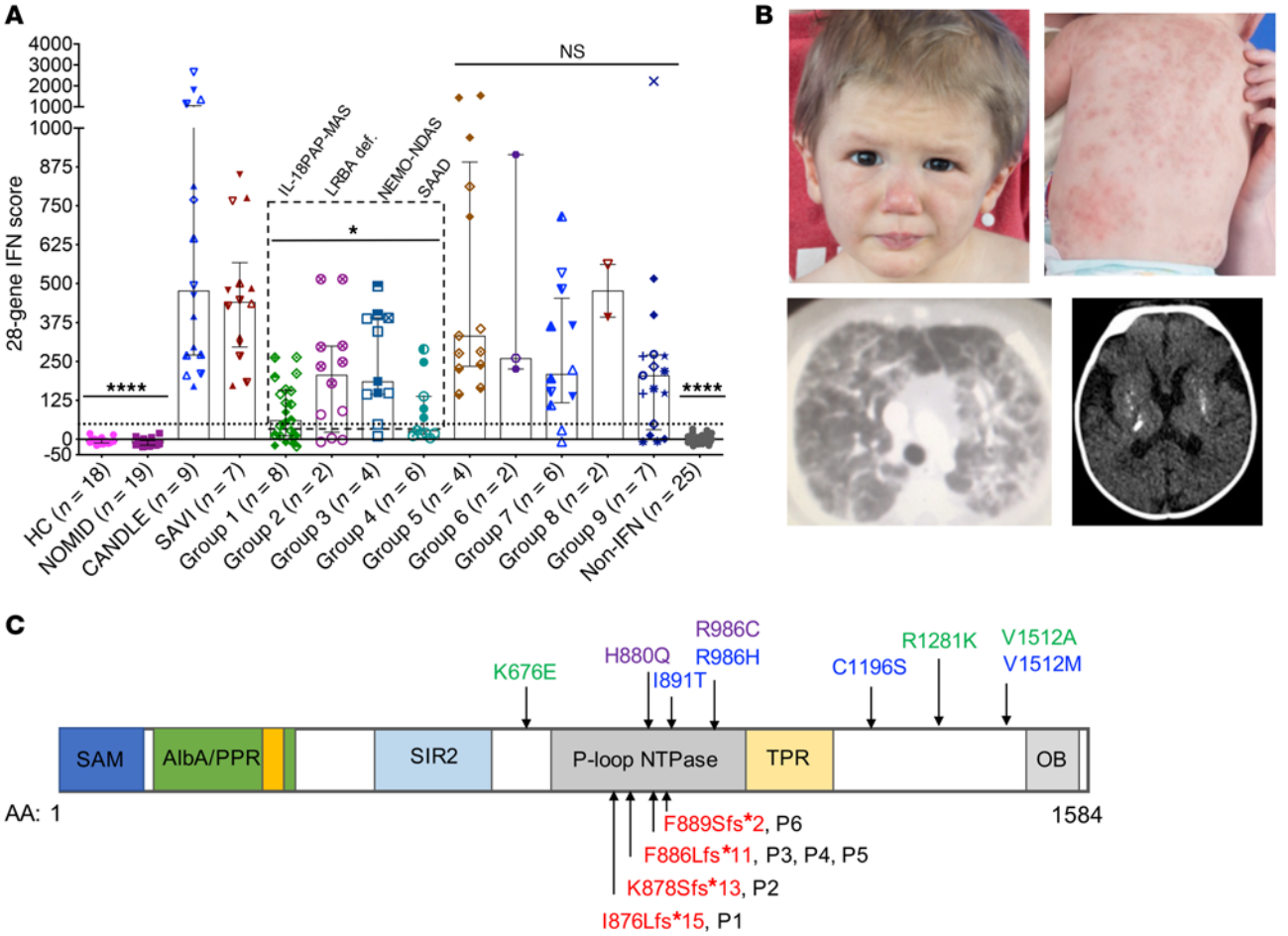

Figure 4. IFN score by disease group and clinical and genetic characteristics of SAMD9L-mediated autoinflammatory disease (SAMD9L-SAAD). (**A**) Twenty-eight–gene IFN scores by disease group. Nonparametric tests were used for multiple comparisons (Kruskal-Wallis) or individual group comparisons (Mann-Whitney). Each patient in groups 1 to 9 (G1 to G9) is represented by a different symbol shape. Depicted in the graph are the statistical significances (Kruskal-Wallis test) from the comparisons of each group (healthy controls [HC], NOMID, G1 to G4 combined, G5, G6, G7, G8, G9, and Non-IFN groups) with CANDLE and SAVI patients combined. *P = 0.0259; ****P < 0.0001; NS, not significant. Bars and error lines indicate median and interquartile range, respectively; dotted line indicates the 28-gene IFN score cutoff (48.9) previously described (34). For the control groups, HC and NOMID, the same symbol is used for different individuals, as only 1 sample per patient is included. For all other disease groups including CANDLE and SAVI, each patient is represented by a different symbol. (**B**) Clinical manifestations of SAMD9L-associated autoinflammatory disease (SAMD9L-SAAD) include nodular panniculitis and lipoatrophy (patient 1), interstitial lung disease (patient 6), and basal ganglia calcifications (patient 5). (**C**) SAMD9L domains and variant localization. SAM (blue), sterile α motif domain; AlbA/PPR (orange/yellow), DNA-binding domain; SIR2 (light blue), silent mating-type information regulator 2; P-loop NTPase (green), P-loop–containing NTP hydrolase; TPR (purple), tetratricopeptide repeat domain; OB (gray), oligonucleotide-binding fold domain; AA, amino acid; P1–P6, patient 1 to patient 6. Variants identified in SAMD9L-SAAD are in red, variants associated with ataxia-pancytopenia syndrome (APS) are in blue, and variants associated with myelodysplastic syndrome (MDS) or acute myeloid leukemia (AML) are in green. Variants associated with either APS or MDS/AML are shown in purple.

patients with *SAMD9L* mutations (G4-P1 and G4-P4) had elevated IRG-S. Of the other 3 patients tested, 2 (G4-P3 and G4-P5) had negative IRG-S and the third patient (G4-P2) had 4 samples tested, 3 with negative IRG-S, and 1 sample, obtained during a rhinovirus induced disease flare, had an elevated IRG-S. Two patients received bone marrow transplants: G4-P3 had received a sibling-matched bone marrow transplant at the age of 20 months, and a second patient (G4-P6) received an allogeneic bone marrow transplant at the age of 9 months.

The highly similar clinical presentation, progressive B cell lymphopenia, and genetic findings (frameshift mutations all within 13 amino acids of each other, absent from public databases, and in a conserved protein domain) support their classification as a previously unrecognized autoinflammatory disease, referred to as SAMD9L-SAAD (G4) (Figure 4, A–C, and Supplemental Table 4).

Potentially novel and known mutations in PRAAS/CANDLE- and AGS-causing genes characterize patients with high IRG-S and suggestive clinical features. Of 4 patients summarized in G5 with neurologic disease manifestations, 2 had spastic quadriplegia and were wheelchair bound (G5-P2 and G5-P3); patient 2 expired in the context of a presumed infection. One patient (G5-P1) who suffered a stroke at the age of 7 years had Moya-Moya–like vasculopathy and was later found to have a previously described (27) homozygous *SAMHD1* deletion. Patient G5-P3 had spastic quadriplegia and peripheral vasculitis. Her father had a very high IRG-S and extensive basal ganglia calcifications

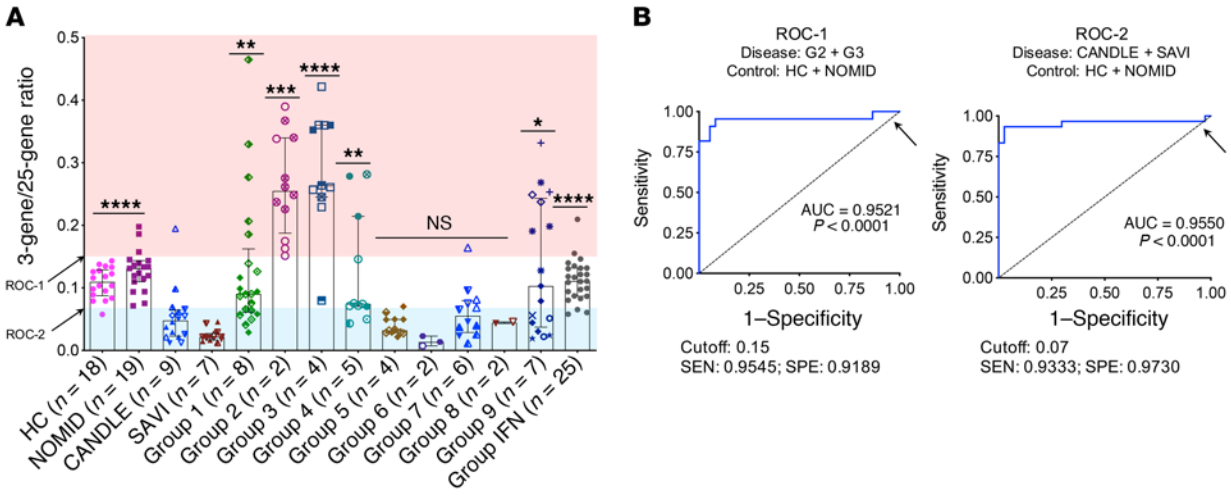

Figure 5. Ratios of 3-gene score (CXCL10 + GBP1 + SOCS1) over 25-gene score (3:25 gene ratio). (**A**) A ratio between 3 IFN-response genes with NF-κB transcription binding sites (CXCL10, GBP1, and SOCS1) and the 25 IFN genes with no NF-κB binding sites (3:25 ratio) was calculated. Depicted in the graph are the statistical significances (nonparametric Kruskal-Wallis test) from the comparisons of each group with CANDLE and SAVI patients combined: healthy controls (HC) and NOMID combined $P < 0.0001$, G1 $P = 0.0017$, G2 $P = 0.0003$, G3 $P < 0.0001$, G4 $P = 0.0027$, G5 $P = 0.9271$, G6 $P = 0.6055$, G7 $P = 0.1499$, G8 $P = 0.8684$, G9 $P = 0.0083$, Non-IFN $P < 0.0001$. NS, not significant. Bars and error lines indicate median and interquartile range, respectively. Red shaded area indicates a high 3:25 gene ratio, blue shaded area indicates low ratio, and white area indicates normal ratio. Cutoffs were calculated in panel **B**. For the control groups (HC and NOMID) the same symbol is used for different individuals, as only one sample per patient is included. In all other groups, including CANDLE and SAVI, each patient is represented by a different symbol. (**B**) Two receiver operating characteristic (ROC) curves for the 3:25 gene ratio to distinguish HC and NOMID from patients with NDAS (G3) and LRBA deficiency (G2) (ROC-1) and CANDLE and SAVI from HC and NOMID (ROC-2) are shown. A black arrow indicates the optimal cutoff (listed under each graph). AUC, area under the curve; SEN, sensitivity; SPE, specificity. The cutoffs for the ROC curves were marked in panel **A** with black arrows on the *y* axis. A list of genes in the IFN-gene score is published in ref. 34. *$P < 0.05$; **$P < 0.01$; ***$P < 0.001$; ****$P < 0.0001$.

during workup of "muscle weakness" and was subsequently included as a patient (G5-P4).

Two patients who suffered from digital ulcerations, interstitial lung disease, and myositis were initially thought to have an autoinflammatory disease, but the presence of anti-MDA5 autoantibodies was consistent with a diagnosis of anti-MDA5 autoantibody–positive JDM. No obvious candidate gene was identified, and these patients (G6-P1 and G6-P2) were grouped together in G6.

Six patients with CANDLE-like features, who had no cytopenias but high IRG-S, were included in G7. Of these, 3 had disease-causing CANDLE mutations (G7-P4 through G7-P6). Patient G7-P4 was homozygous for a known *PSMB8* mutation (p.T75M). Patient G7-P5 was compound heterozygous for 2 potentially novel *PSMB8* mutations (p.S118P and p.Q55*) and patient G7-P6 harbored potentially novel compound heterozygous mutations in the proteasome assembly gene, *PSMG2* (PAC2), that were recently confirmed to be pathogenic (28). Patient G7-P3 had severe localized panniculitis, localized lipoatrophy, and basal ganglia calcifications without white matter disease, and harbored a de novo somatic mutation (~26% allele fraction) in *TREX1* that was previously associated with autosomal dominant AGS1 as a germline mutation (29). Four G7 patients (G7-P3, G7-P4, G7-P5, and G7-P6) were treated with JAK inhibitors with partial or good responses. Patient G7-P4 died due to severe pulmonary hypertension, which developed before initiation of JAK inhibitor treatment (30). Two siblings, G7-P1 and G7-P2, have no genetic diagnosis. G8 includes 2 patients with SAVI-like disease (G8-P1 and G8-P2) who presented with chilblains lesions and systemic inflammation but carried no obvious candidate mutations (Table 2 and Supplemental Table 5).

G9 includes 7 patients with elevated IRG-S who could not be grouped on a clinical, immunological, or genetic basis (Supplemental Table 6).

Patients with negative–IFN-S can be grouped according to clinical phenotype, genotype, and cytokine profile. The findings of the 25 patients with negative IRG-S are described in Supplemental Table 7; these patients could be classified into 4 subgroups (GN1 to GN-4). Five patients had chronic recurrent multifocal osteomyelitis (CRMO) (GN1, $n = 5$). GN1-P2 and GN1-P5 had exclusive jaw involvement and the others had long bone and spine involvement; no unifying genetic hypothesis was found. Four patients had cryopyrin-associated periodic syndrome–like (CAPS-like) disease (GN2, $n = 4$). Interestingly, all had a rare variant of unknown significance in *NLRP3* that was inherited from a parent. All patients in GN2 had complete or partial responses to IL-1–blocking treatment, strengthening the concept that selected low-penetrance variants may predispose to the development of CAPS-like disease (31). No unifying genetic hypothesis was found for 6 patients with periodic fever syndromes (GN3, $n = 6$). Three patients with systemic juvenile idiopathic arthritis–like (sJIA-like) disease and MAS (GN4, $n = 3$) had all high serum IL-18 levels between 9,878 pg/mL and 24,200 pg/mL and IL-18/CXCL9 ratios greater than 1 that have previously been associated with increased risk for the development of MAS (15). Seven patients could not be grouped (GN5, $n = 7$).

Distinct gene expression patterns in 3 NF-κB–coregulated IRGs distinguish disease groups with both NF-κB and IFN signaling for poten-

tial leveraging of the diversity in IRG regulation for diagnostic purposes. Though all disease groups had elevated IRG-S compared with negative controls (healthy controls and NOMID), the mean IRG-S elevation was significantly lower in patients with IL-18PAP-MAS (G1), LRBA deficiency (G2), NEMO-NDAS (G3), and SAMD9L-SAAD (G4). Normalized gene expression for 25 of the 28 IRGs in our assay was significantly higher in CANDLE, SAVI, and disease groups G5–G8 compared with groups G1–G4 except for normalized gene expression in 3 genes, *CXCL10*, *GBP1*, and *SOCS1*, which was equal or higher in groups G1–G4 compared with CANDLE and SAVI (Supplemental Figure 2 and Supplemental Figure 3A).

We hypothesized that the differential expression of these genes may be due to regulation by different transcription factors (TFs). We therefore assessed TF binding sites (TFBSs) in the 28 genes in our IFN score. As expected, all 28 genes have TFBSs for STAT1 and other TFs activated by type-I IFNs. The 3 genes with relatively high expression compared with CANDLE and SAVI in patient groups G1–G4 have additional TFBSs for NF-κB1 (*CXCL10*, *GBP1*, and *SOCS1*) and/or NF-κB2 (*CXCL10*) (Supplemental Figure 3B), thus suggesting that NF-κB–dependent activation of these IRGs may be relatively high in patients in G1–G4 compared with STAT1-dependent activation, which differs in patients with CANDLE and SAVI. To validate a role of NF-κB in driving their expression, we used whole blood RNA-seq data to correlate the expression level of the 3 genes (*CXCL10*, *GBP1*, and *SOCS1*) with that of 11 genes that have NF-κB but no STAT1 TFBSs, by calculating summary *Z* scores, a "3-gene NF-κB/STAT1 score," and an "11-gene NF-κB–only validation score" (Supplemental Methods and Supplemental Figures 3 and 4). The 3-gene NF-κB/STAT1 score did not correlate with the 11-gene NF-κB–only validation score in healthy controls who have no IFN score elevation nor in CANDLE, and SAVI, where we expected predominant type-I IFN/STAT1 inflammation. However, the 11-gene NF-κB–only validation score highly correlated with the 3-gene NF-κB/STAT1 score in patients with LRBA deficiency (G2, $r = 0.82$, $P = 0.02$), NEMO-NDAS (G3, $r = 0.72$, $P = 0.03$), and SAMD9L-SAAD (G4, $r = 0.99$, $P = 0.002$) (Supplemental Figure 5). A "25-gene STAT1-only score" of genes expressing only STAT1 but no NF-κB TFBSs did not correlate with the 11-gene NF-κB–only validation score in any disease group with elevated IRG-S. Interestingly, in the IL-18PAP-MAS patients, neither the 3-gene NF-κB/STAT1 score nor the 25-gene STAT1-only score correlated with the 11-gene NF-κB–only score (G1) (Supplemental Figure 5B). TFs that are activated by recombinant IL-18 (including FOS, ATF2, JUN, and ATF3) (32) were present in the regulatory domains of many of the IRGs in the 28-gene IRG-S (data not shown). In support of the notion that free IL-18 may coregulate the expression of IRGs in patients with IL-18PAP-MAS, we correlated total serum IL-18 levels, which correlates with free IL-18 levels (15), with the IRG-S and found that only serum levels of IL-18 but not IL-18BP and CXCL9 correlated weakly with the 28-gene IRG-S ($r = 0.3$, $P = 0.06$; Supplemental Figure 6A).

A ratio of the 3-gene NF-κB/STAT1 score and the 25-gene STAT1-only score (3:25 ratio) to reflect the relative contribution of NF-κB versus STAT1/IFN–mediated inflammation was very low in CANDLE, SAVI, AGS, AGS-like disease (G5), anti-MDA5 autoantibody–positive JDM (G6), CANDLE/CANDLE-like disease (G7), and SAVI-like disease (G8) (Figure 5A) as well as in childhood systemic lupus erythematosus (SLE) and other JDM (Supplemental Figure 7). A ratio less than 0.07 or greater than 0.15 distinguished the canonical interferonopathies (SAVI or CANDLE) and patients with LRBA deficiency (G2) and with NEMO-NDAS (G3) from healthy controls and NOMID patients, respectively (Figure 5B). The 3:25 ratio was normal in IL-18PAP-MAS. Although most of the 28 IRGs assessed in the IFN score are strongly triggered by type I IFNs, 9 genes are also significantly activated by type II IFN (IFN-γ). Interestingly, a ratio of IFN-γ– and IFN-α– regulated genes over all genes was higher in the IL-18PAP-MAS than in CANDLE and SAVI (Supplemental Figure 6B).

Preliminary outcomes in patients who received treatment with a JAK inhibitor. Although this study was not conducted to collect treatment outcomes, we report preliminary observations to increase available data on these very rare diseases to improve management (Supplemental Table 8). A total of 15 patients have received treatment with JAK inhibitors. Five patients received baricitinib in the context of a compassionate-use study (NCT01724580), and the other 10 patients received a JAK inhibitor through commercial sources: 7 received tofacitinib, 2 ruxolitinib, and 1 baricitinib (Supplemental Table 8). Two patients expired during the period of this study. One patient had anti-MDA5–antibody JDM and received ruxolitinib while on a ventilator for worsening lung disease. The other patient, a CANDLE patient, had severe primary pulmonary hypertension before starting tofacitinib (30). One patient with a psoriasiform dermatitis and scarring skin fibrosis had no response to 9 months of treatment and discontinued baricitinib treatment (G9-P1). Two additional CANDLE patients (G7-P5 and G7-P6) (28) and 1 patient with CANDLE-like disease and a somatic *TREX1* mutation (G7-P3) had complete responses to JAK inhibition and continue on treatment. One patient with AGS5 (G5-P1) was previously reported (33) and has stable disease on baricitinib. Two patients with AGS-like disease had partial to minimal responses to baricitinib and tofacitinib (G5-P3 and G5-P4), respectively, with ongoing significant steroid requirement in 1 patient (G5-P3). Another patient with anti-MDA5 antibody–positive JDM (G6-P1) had a partial response to low dose of tofacitinib with progressive soft tissue and cardiac calcifications. Of the patients in G1–G4 who were treated with a JAK inhibitor, the patient with IL-18PAP-MAS had a partial response with no progression of lung disease and decreasing serum IL-18 levels (G1-P7), and the patient with *LRBA* deficiency has had partial responses with resolving cytopenias and rashes, and lower steroid requirements (G2-P1). One patient with NEMO-NDAS (G3-P4) had a suboptimal response and discontinued tofacitinib. Finally, 1 patient with SAMD9L-SAAD (G4-P1) had a partial response with ongoing skin disease and steroid requirements. Based on our findings, we suggest disease criteria to diagnose patients with and without an elevated IRG-S (Supplemental Table 9).

Discussion

Mendelian autoinflammatory interferonopathies present with chronic elevation of an IRG-S (summarized in ref. 34). Clinical benefit in patients treated with JAK inhibitors who have CANDLE (11), SAVI (11, 35, 36), or AGS (37, 38) are encouraging, and the correlation of treatment responses with suppression of the IRG-S (34) suggests that the IRG-S is useful in diagnosis and as

a biomarker in monitoring treatment responses. In this study, a strategy for screening patients with undifferentiated autoinflammatory diseases that included assessment of IRG-S, cytokine profiling, clinical phenotyping, and genomics led to characterization of additional disease groups of patients with both chronic and temporary IRG-S elevations, and to the development of a ratio of differentially regulated IRGs that were included in a 28-gene score that distinguishes the additional conditions from the canonical interferonopathies, CANDLE, SAVI, and AGS.

Compared with patients with a negative IRG-S, which included patients with osteomyelitis, CAPS-like disease, periodic fever syndromes, and sJIA-like disease with MAS flares and high IL-18 levels, most of which responded to IL-1–blocking treatments, patients with elevated IRG-S had more severe disease and higher mortality, thus underlining the unmet need to find better treatments.

The characterization of patients with clinical phenotypes that resemble CANDLE/PRAAS, who had overall lower IRG-S and developed progressive B cell cytopenias and/or hypogammaglobulinemia, led to the recognition of 3 distinct, monogenic conditions that underline the importance of assessing these mutations in patients suspected to have CANDLE/PRAAS and who are negative for mutations in genes that encode proteasome components. Two patients with CANDLE/PRAAS-like phenotypes had loss-of-function mutations in *LRBA* causing LRBA deficiency (39). Both patients (G2-P1 and G2-P2) had panniculitis and lower CTLA4 surface expression on $CD4^+$ T cells than controls (data not shown), which confirm that the mutations impact CTLA4 recycling (26). However, both patients carry other mutations that may affect IFN signaling (Supplemental Table 4). It therefore remains to be determined whether the IFN signature is a characteristic part of the immune dysregulation of patients with LRBA deficiency (22) or is associated with other rare variants in those patients. Patient G2-P1 is partially responding to JAK inhibition with concomitant decrease in IRG-S after previously unsatisfactory responses to sirolimus and abatacept (Supplemental Table 4), suggesting a possible pathogenic role of increased IFN signaling.

Four patients harbor potentially novel splice variants in *IKBKG*/NEMO, the gamma subunit of the IκB kinase complex that activates NF-κB. In contrast with patients deficient in the NEMO protein who exhibit immunodeficiency, patients with the NEMO spliced mutant who lack only exon 5 (NEMOΔexon5) do not present with severe immunodeficiency but with systemic inflammation panniculitis and elevated IRG-S. Hanson et al. recently explored the molecular mechanisms that coactivate NF-κB and IRGs in these patients and called the disease NEMO-NDAS and found that NEMOΔexon5 stabilizes the TBK1/IKKi complex and facilitates IRF3 phosphorylation, *IFNB1* transcription, and concomitant NF-κB activation. These evaluations provide a potential mechanistic explanation for the type-I IFN–associated "autoinflammatory" clinical features and the concomitant NF-κB nuclear translocation in this previously unrecognized inflammatory syndrome (40).

A severe perinatal-onset inflammatory disease was seen in 6 patients with frameshift mutations in *SAMD9L* that is phenotypically distinct from 2 diseases previously associated with heterozygous missense mutations in *SAMD9L* (41–44). One of the diseases, pancytopenia and ataxia syndrome (41, 44), presents later in life with concomitant cerebellar atrophy and risk of myelodysplasia. Other somatic and selective germline *SAMD9L* mutations can cause pediatric early-onset myelodysplastic syndrome (MDS) (43). The 6 patients reported here harbor potentially novel, de novo frameshift mutations that are in close proximity to each other. The mutations cause immune dysregulation characterized by nodular panniculitis similar to CANDLE/PRAAS, and early-onset interstitial lung disease in most patients (unlike CANDLE/PRAAS), and severe infection-associated myelosuppression/cytopenias. Genetic reversion that is described in pancytopenia and ataxia syndrome (41) and in pediatric MDS (43) was also seen in 1 patient before bone marrow transplant. The inflammatory disease manifestations suggest that these heterozygous *SAMD9L* frameshift mutations confer a gain of function through mechanisms that need to be further investigated. Furthermore, the positive outcome of bone marrow transplantation in 2 of the 6 patients, and the high mortality in patients who have severe concomitant lung disease, point to the importance of distinguishing these patients from CANDLE by making the diagnosis of SAMD9L-SAAD early.

Eight patients uniformly presented with recurrent MAS-like episodes and developed PAP/lipoid pneumonia and clubbing of their distal phalanges. They were diagnosed clinically as having a previously unrecognized disease that is referred to as IL-18PAP-MAS. These patients' histological findings of PAP are distinct from the interstitial fibrosis of SAVI, and are not seen in patients with NLRC4-associated MAS despite comparably high serum IL-18 levels (12, 15). Similarly, elevated IL-18 levels are also seen in some patients with sJIA and adult Still's disease, and are now recognized as factors predisposing to the development of MAS (15, 17, 45–47). Some of these patients are included in a publication that highlights a larger spectrum of sJIA patients who develop a heterogeneous spectrum of lung diseases that include PAP and interstitial lung fibrosis and are referred to as sJIA-LD (48). Patients with IL-18PAP-MAS share a cytokine signature linked to high expression of IL-18 and originally described in NLRC4-MAS (12), which includes hematopoietic growth factors/cytokines like M-CSF, SCF, and IL-3. Interestingly, humanized mice with transgenic expression of human SCF, IL-3, and GM-CSF develop spontaneous MAS directly mediated by myeloid cells (49), raising questions whether IL-18 promotes the production of these growth factors. These mechanisms may synergize with the known function of the role of IL-18 as IFN-γ–stimulating factor in infections and may provide further potential mechanisms by which IL-18 confers MAS susceptibility. The presence of PAP suggests alveolar macrophage dysfunction in clearing surfactant from the alveoli, as is seen in patients with genetic or autoimmune GM-CSF deficiency (50). Whether treatment aimed at blocking IL-18, or IFN-γ signaling, or treatments aimed at modifying phagocytosis and processing of surfactant by alveolar macrophages are viable treatment strategies needs further exploration. Genetic analyses have so far not been conclusive in the IL-18PAP-MAS patients nor the other sJIA-LD patients (48).

Interestingly, the magnitude and pattern of the IRG elevation differed between these 4 conditions (LRBA deficiency, NEMO-NDAS, SAMD9L-SAAD, and IL-18PAP-MAS) versus CANDLE and SAVI. The expression of 3 IRGs that contain both NF-κB and STAT1 TFBSs (*CXCL10, GBP1*, and *SOCS*1) correlated with IFN-independent NF-κB–induced gene expression in LRBA defi-

ciency and NEMO-NDAS, and in SAMD9L-SAAD during flares when IRG-S was elevated, suggesting a relatively large effect of NF-κB signaling, compared with the canonical interferonopathies (CANDLE, SAVI, and AGS) and some autoimmune interferonopathies. Although preliminary, our data suggest that patients with IL-18PAP-MAS, LRBA deficiency, NEMO-NDAS, and SAMD9L-SAAD may have more variable responses to JAK inhibition than CANDLE patients, consistent with the observation that the inflammatory response is complex. The partial response to JAK inhibition would be expected in this scenario and may suggest treatment combinations that target the IFN-mediated and NF-κB–mediated dysregulation. In the IL-18PAP-MAS patients, IRGs induced by IFN-α and IFN-γ relative to those induced by predominantly IFN-α were higher in IL-18PAP-MAS than in the other diseases. The pattern of IRGs did not correlate with NF-κB–induced genes, but correlated weakly with the patients' highly elevated total serum IL-18 levels (often >200,000 pg/mL, whereas normal levels are <500 pg/mL) (15). As any of the IRGs in the 28-gene IRG-S have TFs in their respective regulatory domains that are activated by recombinant IL-18, the correlation of IL-18 levels with the IRG-S suggests that free IL-18 may coregulate the expression of IRGs in patients with IL-18PAP-MAS. IL-18 induces IFN-γ (51), which emerges as a critical downstream mediator of the pathogenesis of MAS (15). Whether and how free IL-18 drives the IRG-S, directly via coregulating expression of IRGs or via promoting IFN-γ needs to be evaluated. Pathomechanisms underlying the promising results with JAK inhibition in MAS and hemophagocytic lymphohistiocytosis (52–54) may be partially attributable to IFN-γ receptor signaling blockade (21), but treatments targeting the IL-18/IFN-γ axis are promising (55).

Overall, this study establishes the value of screening for an interferon signature and for high serum IL-18 levels and expands the diagnostic armamentarium that supports the challenging evaluation of patients with undifferentiated autoinflammatory diseases. The diagnosis of IL-18PAP-MAS, NEMO-NDAS, SAMD9L-SAAD, and LRBA deficiency needs to be considered in patients presenting with elevated IRG-S and clinically suggestive features. A high ratio of 3:25 differentially regulated IRGs identified NEMO-NDAS, LRBA deficiency, and a normal ratio was seen in the SAMD9L-SAAD patients. These diseases mimic CANDLE/PRAAS clinically but higher 3:25 ratios suggest a relatively increased NF-κB signaling distinct from CANDLE/PRAAS and SAVI. Future investigations are necessary to determine whether the 3:25 ratio will be useful in predicting response to IFN-targeted monotherapy, versus the need for additional treatments.

Methods

Patients and healthy controls

Between 2014 and 2017, 66 consecutive patients with presumed undifferentiated autoinflammatory diseases who had no genetic diagnosis upon referral were included in an institutional review board–approved (IRB-approved) natural history study (NCT02974595). All clinical investigations were conducted according to Declaration of Helsinki principles. Written informed consent was obtained from the subjects or their parents either at the NIH or by phone consent. Blood samples were collected from patients and their unaffected family members when available. Healthy controls were recruited through the same study, NCT02974595, and were siblings or family members who have no mutations. For some assays, anonymous healthy blood donors were used.

Clinical, immunological, and genetic evaluation

We assessed 57 patients at the NIH (including physical exam, clinically indicated imaging, and a chest CT) and immunologically (T, B, NK cell count, immunoglobulins, and rheumatologic work up). Five patients passed away before an NIH visit could be arranged, and in 4 patients logistical problems precluded travel to the NIH. Samples for genetic testing were obtained from all 66 patients either at the NIH or were sent under NCT02974595. WES was performed in 19 trios, 1 duo, and 4 singletons, whole-genome sequencing (WGS) in 36 trios and 1 duo; 5 patients had Sanger sequencing of candidate genes performed only. Confirmatory targeted (Sanger) sequencing of candidate genes detected by WES or WGS was performed. Next-generation sequencing data are registered in NCBI's dbGaP database (https://www.ncbi.nlm.nih.gov/gap/) under accession number phs001946.v1.p1.

Cytokine analysis

Serum was collected from 53 of 66 patients and 5 healthy controls. Cytokine concentrations of 48 analytes were measured using the Bio-Plex system (Bio-Rad) (3) in 2 batches. Cytokine analysis was done in 28 of the 36 patients with elevated IFN signature (presumed undifferentiated interferonopathy [UIFN]). The first batch included 45 patients, 20 with UIFN and 25 without UIFN, and 5 healthy controls, and the second batch included 8 patients with an UIFN. Due to a ceiling effect of high serum IL-18 levels in the Bio-Plex system, all samples with levels greater than 10,000 pg/mL were re-run in a dedicated ELISA assay, as previously described (15). All patients with a history of MAS had serum measurements that included IL-18, IL-18BP, and CXCL9 (MIG) as described in Weiss et al. (15).

NanoString 28-gene IRG-S

At least 1 IRG-S was obtained for 65 of 66 patients. It was not obtained from 1 patient with a *SAMD9L* mutation (G4-P5). As previously reported, total RNA was extracted from blood samples collected in Paxgene tubes (Qiagen). Gene expression of selected IRGs was determined by NanoString (NanoString Technologies) and an IRG-S was calculated as previously described based on healthy control data (34).

Within the 28 IRGs of the NanoString IRG-S, 3 IRGs were identified as having an *NFKB1* and/or an *NFKB2* TFBS. For validation and correlation of a 3-gene subscore of IRGs with STAT1 and NF-κB1 and NF-κB2 TFBSs with other genes preferentially activated by NF-κB1 and NF-κB2 that lack STAT1 binding sites, please refer to Supplemental Methods D, Supplemental Figure 3B, and Supplemental Figure 4, A and B.

Evaluation of the 3-gene to 25-gene ratio (3:25 ratio) in the various diseases. A ratio of the sum of the normalized counts of the 3 NanoString ISGs with NF-κB binding sites (*CXCL10*, *GBP1*, and *SOCS1*) and the sum of the normalized counts of the 25 other genes was generated and compared between diseases.

Statistics

Descriptive analyses were performed; no adjustments for multiple comparisons were made. For normally distributed data, parametric tests (unpaired 2-tailed *t* tests for group comparison, i.e., cytokine

analysis) were used. Nonparametric tests were used for not normally distributed data (Kruskal-Wallis for multiple comparisons and Mann-Whitney test for group comparison). Pearson's correlation was used for correlations of the 3-, 11-, and 25-gene subscores. Receiver-operating characteristic (ROC) curves were generated comparing the 3-gene/25-gene ratio in CANDLE and SAVI versus the various disease groups (G1–G9) to healthy controls and NOMID samples using the Wilson-Brown method; a confidence interval of 95% is reported. *P* values below 0.05 were considered statistically significant for all tests performed. All statistical analyses described above were performed using GraphPad Prism version 8.00 for Mac OS.

Study approval

The study was approved by IRBs at the NIH, NIAID. All patients were enrolled in the NIH Natural History Protocol of Autoinflammatory Diseases (NCT02974595). Patients or their parents provided written informed consent. Additional written photo consent was obtained from patients included in this paper. Most patients were evaluated at the NIH. Patients unable to come to the NIH were consented over the telephone and blood samples for RNA and DNA analysis as well as medical records were sent to the NIH.

Author contributions

AAJ and GAMS acquired data, oversaw the clinical aspects of the study, and analyzed data. Members of the Autoinflammatory Diseases Network referred patients and acquired and interpreted clinical data. LM, AB, YH, BM, and SM conducted experiments, and acquired and analyzed data. SC acquired and analyzed clinical and biomarker subspecialty data. AJO oversaw the statistical analyses of the study data. YH and GAMS acquired clinical data. KRC interpreted clinical and bone marrow biopsy data. SB and ZD analyzed genetic data. AAJ and RGM designed the study, analyzed the data, and wrote the first draft of the manuscript. Authors listed in the Autoinflammatory Disease Consortium (AA to TWM) provided critical patient information and phenotyping data. All authors reviewed and approved the final version of the manuscript.

Acknowledgments

We would like to thank Samantha Dill, Dawn Chapelle, and Laura Failla for excellent patient care; and Nicole Plass, Wendy Goodspeed, Michelle O'Brian, and Susan Pfeiffer for scheduling patients. We would also like to thank Jacob Mitchell and Rachel VanTries for running experiments. We further thank Paul Wakim for his review and advice on the statistical aspects of the correlation analyses. Funding was provided by the Intramural Research Program of the NIH, NIAID, NIAMS, and the Clinical Center.

Address correspondence to: Adriana A. de Jesus or Raphaela Goldbach-Mansky, Translational Autoinflammatory Diseases Section (TADS)/LCIM/NIAID, NIH, Building 10 Room 11C215 (AAJ) or Room 11C205 (RGM) MSC 1888, 10 Center Drive, Bethesda, Maryland 20892-1888, USA. Phone: 301.761.7768; Email: adriana.almeidadejesus@nih.gov (AAJ). Phone: 301.761.7553; Email: goldbacr@mail.nih.gov (RGM).

1. de Jesus AA, Canna SW, Liu Y, Goldbach-Mansky R. Molecular mechanisms in genetically defined autoinflammatory diseases: disorders of amplified danger signaling. *Annu Rev Immunol*. 2015;33:823–874.
2. Brehm A, et al. Additive loss-of-function proteasome subunit mutations in CANDLE/PRAAS patients promote type I IFN production. *J Clin Invest*. 2015;125(11):4196–4211.
3. Liu Y, et al. Activated STING in a vascular and pulmonary syndrome. *N Engl J Med*. 2014;371(6):507–518.
4. Bennett L, et al. Interferon and granulopoiesis signatures in systemic lupus erythematosus blood. *J Exp Med*. 2003;197(6):711–723.
5. Liu Y, et al. Mutations in proteasome subunit β type 8 cause chronic atypical neutrophilic dermatosis with lipodystrophy and elevated temperature with evidence of genetic and phenotypic heterogeneity. *Arthritis Rheum*. 2012;64(3):895–907.
6. Yang YG, Lindahl T, Barnes DE. Trex1 exonuclease degrades ssDNA to prevent chronic checkpoint activation and autoimmune disease. *Cell*. 2007;131(5):873–886.
7. Stetson DB, Ko JS, Heidmann T, Medzhitov R. Trex1 prevents cell-intrinsic initiation of autoimmunity. *Cell*. 2008;134(4):587–598.
8. Volkman HE, Stetson DB. The enemy within: endogenous retroelements and autoimmune disease. *Nat Immunol*. 2014;15(5):415–422.
9. Crow YJ, et al. Mutations in the gene encoding the 3'-5' DNA exonuclease TREX1 cause Aicardi-Goutières syndrome at the AGS1 locus. *Nat Genet*. 2006;38(8):917–920.
10. Lebon P, Meritet JF, Krivine A, Rozenberg F. Interferon and Aicardi-Goutières syndrome. *Eur J Paediatr Neurol*. 2002;6(suppl A):A47–A53.
11. Sanchez GAM, et al. JAK1/2 inhibition with baricitinib in the treatment of autoinflammatory interferonopathies. *J Clin Invest*. 2018;128(7):3041–3052.
12. Canna SW, et al. An activating NLRC4 inflammasome mutation causes autoinflammation with recurrent macrophage activation syndrome. *Nat Genet*. 2014;46(10):1140–1146.
13. Romberg N, et al. Mutation of NLRC4 causes a syndrome of enterocolitis and autoinflammation. *Nat Genet*. 2014;46(10):1135–1139.
14. Bracaglia C, et al. Elevated circulating levels of interferon-γ and interferon-γ-induced chemokines characterise patients with macrophage activation syndrome complicating systemic juvenile idiopathic arthritis. *Ann Rheum Dis*. 2017;76(1):166–172.
15. Weiss ES, et al. Interleukin-18 diagnostically distinguishes and pathogenically promotes human and murine macrophage activation syndrome. *Blood*. 2018;131(13):1442–1455.
16. Girard-Guyonvarc'h C, et al. Unopposed IL-18 signaling leads to severe TLR9-induced macrophage activation syndrome in mice. *Blood*. 2018;131(13):1430–1441.
17. Wada T, et al. Sustained elevation of serum interleukin-18 and its association with hemophagocytic lymphohistiocytosis in XIAP deficiency. *Cytokine*. 2014;65(1):74–78.
18. Gernez Y, et al. Severe autoinflammation in 4 patients with C-terminal variants in cell division control protein 42 homolog (CDC42) successfully treated with IL-1β inhibition. *J Allergy Clin Immunol*. 2019;144(4):1122–1125.e6.
19. Okamura H, et al. Cloning of a new cytokine that induces IFN-gamma production by T cells. *Nature*. 1995;378(6552):88–91.
20. Gabay C, et al. Open-label, multicentre, dose-escalating phase II clinical trial on the safety and efficacy of tadekinig alfa (IL-18BP) in adult-onset Still's disease. *Ann Rheum Dis*. 2018;77(6):840–847.
21. Lounder DT, Bin Q, de Min C, Jordan MB. Treatment of refractory hemophagocytic lymphohistiocytosis with emapalumab despite severe concurrent infections. *Blood Adv*. 2019;3(1):47–50.
22. Gámez-Díaz L, et al. The extended phenotype of LPS-responsive beige-like anchor protein (LRBA) deficiency. *J Allergy Clin Immunol*. 2016;137(1):223–230.
23. Esposito DL, et al. A novel T608R missense mutation in insulin receptor substrate-1 identified in a subject with type 2 diabetes impairs metabolic insulin signaling. *J Clin Endocrinol Metab*. 2003;88(4):1468–1475.
24. Esposito DL, et al. Deletion of Gly723 in the insulin receptor substrate-1 of a patient with non-insulin-dependent diabetes mellitus. *Hum Mutat*. 1996;7(4):364–366.
25. German JP, et al. Leptin deficiency causes insulin resistance induced by uncontrolled diabetes. *Diabetes*. 2010;59(7):1626–1634.
26. Lo B, et al. Autoimmune disease. Patients with LRBA deficiency show CTLA4 loss and immune dysregulation responsive to abatacept therapy. *Science*. 2015;349(6246):436–440.
27. Leshinsky-Silver E, et al. A large homozygous deletion in the SAMHD1 gene causes atypical

Aicardi-Goutiéres syndrome associated with mtDNA deletions. *Eur J Hum Genet*. 2011;19(3):287–292.
28. de Jesus AA, et al. Novel proteasome assembly chaperone mutations in PSMG2/PAC2 cause the autoinflammatory interferonopathy CANDLE/PRAAS4. *J Allergy Clin Immunol*. 2019;143(5):1939–1943.e8.
29. Rice G, et al. Heterozygous mutations in TREX1 cause familial chilblain lupus and dominant Aicardi-Goutieres syndrome. *Am J Hum Genet*. 2007;80(4):811–815.
30. Buchbinder D, Montealegre Sanchez GA, Goldbach-Mansky R, Brunner H, Shulman AI. Rash, fever, and pulmonary hypertension in a 6-year-old female. *Arthritis Care Res (Hoboken)*. 2018;70(5):785–790.
31. Kuemmerle-Deschner JB, et al. Clinical and molecular phenotypes of low-penetrance variants of NLRP3: diagnostic and therapeutic challenges. Arthritis Rheumatol. 2017;69(11):2233–2240.
32. Kanda N, Shimizu T, Tada Y, Watanabe S. IL-18 enhances IFN-gamma-induced production of CXCL9, CXCL10, and CXCL11 in human keratinocytes. *Eur J Immunol*. 2007;37(2):338–350.
33. Sanchez GAM, et al. JAK1/2 inhibition with baricitinib in the treatment of autoinflammatory interferonopathies. *J Clin Invest*. 2018;128(7):3041–3052.
34. Kim H, et al. Development of a validated interferon score using NanoString technology. *J Interferon Cytokine Res*. 2018;38(4):171–185.
35. König N, et al. Familial chilblain lupus due to a gain-of-function mutation in STING. *Ann Rheum Dis*. 2017;76(2):468–472.
36. Frémond ML, et al. Efficacy of the Janus kinase 1/2 inhibitor ruxolitinib in the treatment of vasculopathy associated with TMEM173-activating mutations in 3 children. *J Allergy Clin Immunol*. 2016;138(6):1752–1755.
37. Meesilpavikkai K, et al. Efficacy of baricitinib in the treatment of chilblains associated with Aicardi-Goutieres syndrome, a type I interferonopathy. *Arthritis Rheumatol*. 2019;71(5):829–831.
38. Vanderver A, et al. Open label use of the Janus kinase inhibitor baricitinib in a genetic interferonopathy, Aicardi Goutières syndrome. *Ann Neurol*. 2019;86(supplement 23). https://onlinelibrary.wiley.com/doi/epdf/10.1002/ana.25559.
39. Lopez-Herrera G, et al. Deleterious mutations in LRBA are associated with a syndrome of immune deficiency and autoimmunity. *Am J Hum Genet*. 2012;90(6):986–1001.
40. Wessel AWH, et al. Inflammatory disease and an impaired type I interferon response resulting from a de novo human NEMO hypomorphic mutation. Arthritis and Rheumatology Abstract Supplement 2013 Annual Meeting. 2013;65(10 supplement):S323. https://onlinelibrary.wiley.com/doi/epdf/10.1002/art.38216.
41. Tesi B, et al. Gain-of-function *SAMD9L* mutations cause a syndrome of cytopenia, immunodeficiency, MDS, and neurological symptoms. *Blood*. 2017;129(16):2266–2279.
42. Nagata Y, et al. Germline loss-of-function *SAMD9* and *SAMD9L* alterations in adult myelodysplastic syndromes. *Blood*. 2018;132(21):2309–2313.
43. Pastor VB, et al. Constitutional *SAMD9L* mutations cause familial myelodysplastic syndrome and transient monosomy 7. *Haematologica*. 2018;103(3):427–437.
44. Chen DH, et al. Ataxia-Pancytopenia syndrome is caused by missense mutations in SAMD9L. *Am J Hum Genet*. 2016;98(6):1146–1158.
45. Ichida H, et al. Clinical manifestations of adult-onset Still's disease presenting with erosive arthritis: Association with low levels of ferritin and interleukin-18. *Arthritis Care Res (Hoboken)*. 2014;66(4):642–646.
46. Mazodier K, et al. Severe imbalance of IL-18/IL-18BP in patients with secondary hemophagocytic syndrome. *Blood*. 2005;106(10):3483–3489.
47. Shimizu M, Nakagishi Y, Yachie A. Distinct subsets of patients with systemic juvenile idiopathic arthritis based on their cytokine profiles. *Cytokine*. 2013;61(2):345–348.
48. Schulert GS, et al. Systemic Juvenile idiopathic arthritis-associated lung disease: characterization and risk factors. *Arthritis Rheumatol*. 2019;71(11):1943–1954.
49. Wunderlich M, et al. A xenograft model of macrophage activation syndrome amenable to anti-CD33 and anti-IL-6R treatment. *JCI Insight*. 2016;1(15):e88181.
50. Suzuki T, Trapnell BC. Pulmonary alveolar proteinosis syndrome. *Clin Chest Med*. 2016;37(3):431–440.
51. Bohn E, et al. IL-18 (IFN-gamma-inducing factor) regulates early cytokine production in, and promotes resolution of, bacterial infection in mice. *J Immunol*. 1998;160(1):299–307.
52. Sin JH, Zangardi ML. Ruxolitinib for secondary hemophagocytic lymphohistiocytosis: First case report. *Hematol Oncol Stem Cell Ther*. 2019;12(3):166–170.
53. Broglie L, et al. Ruxolitinib for treatment of refractory hemophagocytic lymphohistiocytosis. *Blood Adv*. 2017;1(19):1533–1536.
54. Zandvakili I, Conboy CB, Ayed AO, Cathcart-Rake EJ, Tefferi A. Ruxolitinib as first-line treatment in secondary hemophagocytic lymphohistiocytosis: A second experience. *Am J Hematol*. 2018;93(5):E123–E125.
55. Prencipe G, Bracaglia C, De Benedetti F. Interleukin-18 in pediatric rheumatic diseases. *Curr Opin Rheumatol*. 2019;31(5):421–427.